Numerical investigation of two-phase flow in high-permeability porous media Effect of permeability variation on traction terms

Maxime Cochennec[1]

Hossein Davarzani[1]* (h.davarzani@brgm.fr) Yohan Davit[2]

Ioannis Ignatiadis[1] Michel Quintard[2]

March 23, 2020

[1]French Geological Survey, Orléans, France [2]Institut de Mécanique des Fluides de Toulouse, Toulouse, France

*To whom correspondence should be addressed

Abstract

In this paper we study the effects of varying permeability on traction terms exerted at the different boundaries for two-phase flow in Hele-Shaw cell. The traction terms, or surface force, are surface integrals that are necessary to close the continuous macroscopic momentum balance equations for two-phase flow in porous media. These terms are usually modeled from experimental results

or obtained by solving a closure problem (a set of boundary value problems to solve on a representative periodic unit-cell). Here these terms are calculated directly by means of direct numerical simulations, and the value of these terms on each interface is studied as a function of the varying permeability and capillary number. We focus on two-phase displacement in high-permeability porous media for which the characteristic flow regimes implies a non-negligible extent of the fluid-fluid interface and thus;

Introduction

Two-phase flow in high-permeability porous media

An accurate description of two-phase flow in high-permeability porous media is of major importance for several practical applications. One can mention, among others, soil remediation in gravely soils [1], nuclear safety [2] or hydrodynamic of catalytic fixed bed reactors [3]. However, most of the literature is dedicated to two-phase flow in low-permeability porous media.

Due to the larger pore size, two-phase flow in high-permeability porous media (hereafter, high-permeability porous media refers to media for which the characteristic particle diameter is about one millimeter and above) results in a complex interaction between capillary, gravity and viscous forces [4]. Because of this complex interplay, the characteristic flow regimes are very different from those observed for surface tension dominated flow [5]. For low-permeability medium, if the surface tension between the fluids is not too low and the viscosity not too high, that is the capillary number is low (usually inferior to 10^{-3}), the fluid repartition pattern is described as two independent flow streams separate by a multitude of stable meniscus at steady state, as illustrated in fig. 1 (a). In this case, for a completely wet medium, the wetting phase flows in the small

pores while the non-wetting phase tends to occupy the larger pores. For high permeability porous media, the fluid velocity can be high enough that the viscous forces dominate over capillary forces (alike gravity and inertial effects may become important if Bond and Reynolds numbers are high, respectively). Then, the fluids repartition patterns can take two forms, either the non-wetting phase is continuous, see for example fig. 1 (b), or is flowing as droplets or ganglia as in fig. 1 (c), while the wetting phase is flowing as a film in contact with the solid. In both cases, the two fluids occupy most of the pores at the same time and the non-wetting phase flows at the center of the pores surrounded by the wetting phase. One can note that these flow regimes are equivalent to those observed in two-phase flows in a tube (slug flow, bubbly flow). Strictly speaking, these different regimes must be considered when attempting to describe two-phase flows with continuous macroscopic equations. Indeed, it has been shown on numerous works that the overall flow depends on the flow regimes [6,7]. In the first glance, one would consider that the exchange terms between the fluid phases as negligible compared to their counterpart between the fluid phases and the solid phase for surface-tension dominated flwo and that the extent of the fluid-fluid interface is small, as in fig. 1 (a). On the other hand, and this is what we are interested in here, this is not necessarily the case for regimes specific to flow in high-permeability porous media for which the extent of the fluid-fluid interface is large. This is important because, as we will see in the next section, these exchange terms between phases are the basis of any attempt to establish continuous relationships on a macroscopic scale starting from the pore scale.

Continuous model

Here we present two different approaches to treat the continuous macroscopic momentum equations for two-phase flow. Although fundamentally identical,

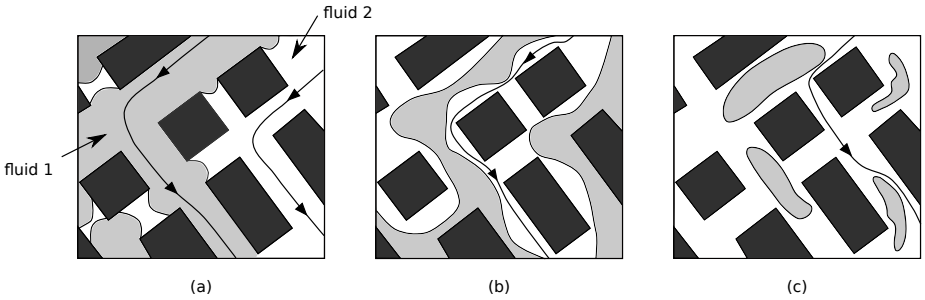

Figure 1: Illustration of possible fluids dispatching in a 2D porous network with solid phase in black, fluid 1, that stands for the non-wetting phase (gray) and the wetting fluid (white), (a) the two fluids are flowing in different channels separate by numerous meniscus (b) wetting and non-wetting fluid are flowing together in most of the pores as two continuous streams and (c) both fluids are flowing together in most of the pores and the non-wetting phase is discontinuous - Adapted from [5]

these approaches were developed for the needs of two different specialties, namely, the study of groundwater flows and the study of the hydrodynamic of chemical reactors.

Porous media approach

The ubiquitous continuous model used to describe two-phase flows in soils is based on an extension of the Darcy equation (creeping saturated single-phase flow in porous media). The whole model, also known as Muskat equations [8,9], reads

$$0 = \frac{\partial \varepsilon S_i}{\partial t} + \nabla \cdot \mathbf{U}_i, \quad i = o, w, \tag{1}$$

$$\mathbf{U}_i = -\frac{1}{\mu_i}\mathbf{K}_i \cdot (\nabla P_i - \rho_i \mathbf{g}), \quad i = o, w, \tag{2}$$

$$1 = S_w + S_o \tag{3}$$

$$\mathbf{K}_w = \mathbf{K}k_{rw}(S_w), \qquad \mathbf{K}_o = \mathbf{K}k_{ro}(S_w), \tag{4}$$

$$P_c(S_w) = P_o - P_w. \tag{5}$$

In these equations, the subscripts o and w refer to the non-wetting and wetting phase, respectively. S_i is the saturation of phase i, ε is the medium porosity, $\mathbf{U}_i$ is the superficial mean velocity of fluid i, P_i is the intrinsic mean pressure of fluid i and $\mathbf{K}$ is the absolute permeability tensor. The generalization toward two-phase flows involves the introduction of the relative permeability terms k_{ri} which account for one phase for the inaccessible void space occupied by the other fluid [5]. To close the set of the macroscopic equations, the relative permeabilities are assumed to be non-linear functions of the saturation and a relation between the macroscopic pressure of each fluid has to be furnished. This relation, is known as the capillary pressure relation and, as for the relative permeabilities, is supposed to vary non-linearly with the saturation only [10].

A significant amount of work attempted to make improvements to the Muskat equations (e.g. including moving contact line [11–13] or take into account the trapped phases [14]). Here we would stress that the concept of relative permeabilities into the Muskat equations is dedicated to independent flow pathways only [15] and the underlying assumption that the two streams do not interfere with each other. However, in case that the area of the fluid-fluid interface is not negligible compared to the solid-fluid interface, as for flow regimes fig. 1 (b) and fig. 1 (c), one would include supplementary terms dedicated to the

momentum exchange across the fluid-fluid interface due to normal and shear stresses exerted on it (i.e. coupling between the phases) into the macroscopic momentum equations. In fact, it has been theoretically established that the macroscopic equations of motion obtained by averaging of the Stokes equations contain momentum exchange terms between fluids [16–19]. The volume averaged momentum equation for the i-phase read

$$0 = -\varepsilon_i \nabla P_i + \varepsilon_i \rho_i \mathbf{g} + \frac{1}{V} \int_{A_{is}+A_{ij}} \mathbf{n}_i \cdot \left(-\mathbf{I} p_i + \mu_i \left(\nabla \mathbf{u}_i + (\nabla \mathbf{u}_i)^T \right) \right) \mathrm{d}A. \quad (6)$$

The next step in the upscaling methods literature is to express the boundaries integral of exchange between the phases in terms of averaged quantity through the resolution of boundary value problems on a representative periodic unit-cell. We need to go no further here but we insist that, as shown in [20], once the closure problems have been solved, the macroscopic equations of motion can be put into a form analogous to the generalized Darcy's law,

$$\mathbf{U}_i = -\frac{1}{\mu_i} \mathbf{K}^*_{ii} \cdot (\nabla P_i - \rho_i \mathbf{g}) - \frac{1}{\mu_j} \mathbf{K}^*_{ij} \cdot (\nabla P_j - \rho_j \mathbf{g}), \quad i, j = o, w \text{ and } i \neq j, \ (7)$$

in which $\mathbf{K}^*_{ij}$ are the coupled relative permeability tensors.

Many studies have attempted to calculate coupled permeabilities experimentally based on the eq. 7, but before we turn to present results from the literature, we discuss the chemical engineering point of view on the continuous model.

Chemical engineering approach

CFD modeling applied to the hydrodynamics of trickle-bed reactors (TBR) is in most cases focused on an Euler-Euler flow formulation. The two fluids are thus treated as two interpenetrating continua. The volume averaged momentum equation for the two fluids to solve, taking into account that the inertial effects are not negligible here, read

$$\rho_i \varepsilon_i \left(\frac{\partial \mathbf{U}_i}{\partial t} + \mathbf{U}_i \cdot \nabla \mathbf{U}_i \right) = -\varepsilon_i \nabla P_i + \varepsilon_i \rho_i \mathbf{g} + \mathbf{F}_{mi} + \varepsilon_i \nabla \cdot \boldsymbol{\tau}_i + \nabla \cdot \mathbf{R}_i, \quad (8)$$

where ε_i is the volume fraction of phase i, the velocity and the pressure are averaged quantities identical to the generalized Darcy equations, $\boldsymbol{\tau}_i$ denotes the viscous stress tensor and $\mathbf{R}_i$ is the pseudo-turbulence stress. The vectors $\mathbf{F}_{mi}$ are the momentum transfer terms at the interface for the i-phase. These terms have to be expressed in terms of constitutive relation to close the set of equations, and the main difference between the existing continuous models is the choice of correlations used for these terms. We stress here that the two equations eq. 6 and +**???** are equivalents (except for the non-linear inertial terms).

Modeling of the momentum exchange between fluids

Here we present different estimation of the momentum transfer terms (i.e. coupled relative permeabilities in the porous media framework) between fluids. Based on the generalized Darcy law with cross terms eq. 7, experimental works computed the coupled transport coefficient through steady-state cocurent flow in sandpack with alternatively one fluid, then the other, which is submitted to a null pressure gradient. This protocol was used with oil and water in a cylindric sandpack [21] and the authors found a negligible effect of the coupled permeabilities in the

overall flow. With the same protocol, with oil and water in a 2D-sandpack Dullien and Dong [22] found that the coupled permeabilities are important since they can contribute at best to 35% of the effective permeability. Alternatively, authors imposed [23] a null displacement and measured the induced pressure drop, with air and water in a Berea sandstone core they found that the coupled transport coefficients must not be overlooked for intermediate saturations. Several authors conducted experiments with two different set-ups as proposed by Rose [24], e.g. [25], in which the authors made cocurrent and countercurrent experiments with water and oil in a sandpack and found that coupled permeabilities reach, at least, 15% of the effective permeability value. However, it was pointed out that the saturation between the two sets of experiments can be very different and therefore the computed relative permeabilities can not be safely compared [26]. The effect of the non-wetting phase connectivity on the transport parameters was extensively studied in [27], the authors performed steady-state cocurrent two-phase flow in 2D-micro model experiments and found that the contribution of the coupled permeabilities on the flow is non-negligible and depend on the flow regimes.

Several numerical studies investigate the share of the coupled permeabilities in the effective permeability. The seminal work of Rothman [28] examined the question by conducting two-phase flow simulations in simple geometries with the immiscible lattice-gas method. The author found non-negligible participation of the coupled permeabilities by applying the volume force alternatively on each fluid. Numerous authors used the lattice-Boltzmann method, such as [29], in which the authors examined the value of the coupled permeabilities as a function of the saturation in a 3D-sphere pack and they found results in agreement with Rothman's results. In [30] the authors used a lattice Boltzmann method in 2D and 3D pore networks and found a non-wetting apparent relative permeability

greater than unity when the wetting fluid is more viscous than the non-wetting fluid. This result is a manifestation of the lubrification effect, also observed in experiments [31], and arising because of a strongly hydraulic coupling between the fluids. Recently, in [32], the authors have used a Volume Of Fluid method to study the transport coefficients of fluid layers in non-circular capillary tubes. Based on analogy with a model Couette flow the authors have derived simple relations that can predict with good accuracy the transport coefficients of fluid layers.

Outline of the study

In this study, we investigate the effect of the varying intrinsic permeability and capillary number on the momentum transfer terms through direct numerical simulations of two-phase flow in a model high-permeability 2D-porous media. To do so we compute the surface integrals in eq. 6 on each boundaries of the system. The idea of solving a depth-averaged flow in a Hele-Shaw allows us to introduce an additional permeability term and thus to vary the intrinsic permeability of the strucure without having to modify the geometry per se.

Theoretical background

Macroscopic quantities

In the following, the superficial mean of a physical quantity θ_i associated with the i-phase is given by

$$\langle \theta_i \rangle = \frac{1}{V} \int_{V_i} \theta_i \, \mathrm{d}V. \tag{9}$$

Macroscopic quantities such as saturation and intrinsic mean pressure for two

fluids $i = w, o$ read

$$S_i = \frac{1}{V} \int_V \chi_i \, \mathrm{d}V \tag{10}$$

and

$$P_i = \frac{\int_V p\chi_i \, \mathrm{d}V}{\int_V \chi_i \, \mathrm{d}V}, \tag{11}$$

respectively. In these equations V is the volume accessible to the fluids, that is the pore volume, and χ_i is the phase indicator of the i-fluid (scalar function that takes the value 1 in the fluid and 0 elsewhere). The quantity $\int_V \chi_i \, \mathrm{d}V$ is the volume fraction of the i-fluid that is ε_i as already introduced in the previous section.

Then we can introduce the dynamic capillary pressure defined as the difference of the intrinsic mean pressures,

$$P_c = P_o - P_w. \tag{12}$$

Traction terms

As previously said, an essential step in order to derive some macroscopic law at macroscale from the microscale is to use averaged quantities to express the momentum transfer terms between phases that arising because of the averaging theorem application [33]. Remember that these closure relations are not presented here but rather we leave intact the surface integrals, the averaged momentum balance equations eq. 6 for two fluids w and o, are recast as

$$0 = -\varepsilon_w \nabla P_w + \mathbf{T}_{wo} + \mathbf{T}_{ws},$$

$$0 = -\varepsilon_o \nabla P_o + \mathbf{T}_{ow} + \mathbf{T}_{os},$$

where ε_i and P_i are the macroscopic quantities defined above, $\mathbf{T}_{ij}$ the traction (name given to surface forces in the Boundary Integral Methods literature in which these integrals are central) exerted by the i-fluid on the j-fluid and $\mathbf{T}_{is}$ the traction exerted by the i-fluid on the solid surfaces [34]. The traction terms are written as

$$\mathbf{T}_{ij} = \frac{1}{V} \int_{A_{ij}} \mathbf{n}_{ij} \cdot (-p_i \mathbf{I} + 2\mu_i \mathbf{e}_i) \, \mathrm{d}A,$$

where $\mathbf{n}_{ij}$ is the normal vector at the interface and pointing toward the j-phase, p_i the pointwise pressure of the i-fluid and $\mathbf{e}_i = \frac{1}{2}\left(\nabla \mathbf{u}_i + (\nabla \mathbf{u}_i)^T\right)$ the rate-of-strain tensor for Newtonian fluids with $\mathbf{u}_i$ the pointwise velocity of the i-fluid.

Theory of two-phase displacement in Hele-Shaw cell

Two-phase flow between two parallel plates under study here is depicted in fig. 2. This illustration represents a cocurrent flow of two fluids inside a Hele-Shaw cell parallel to the $x - y$ plane, with the z-axis perpendicular to the plates, and for which h is the aperture between the plates. A solid obstacle of circular cross-section is sandwiched between the two plates. Tangential (cell plane) stress, as well as stress arising from the perpendicular confinement, need to be taking into account to properly describe the flow. The important parameter here are the aspect ratio h/l where l is some characteristic transverse length (hereafter l is the cell width as shown in fig. 2) and the capillary number.

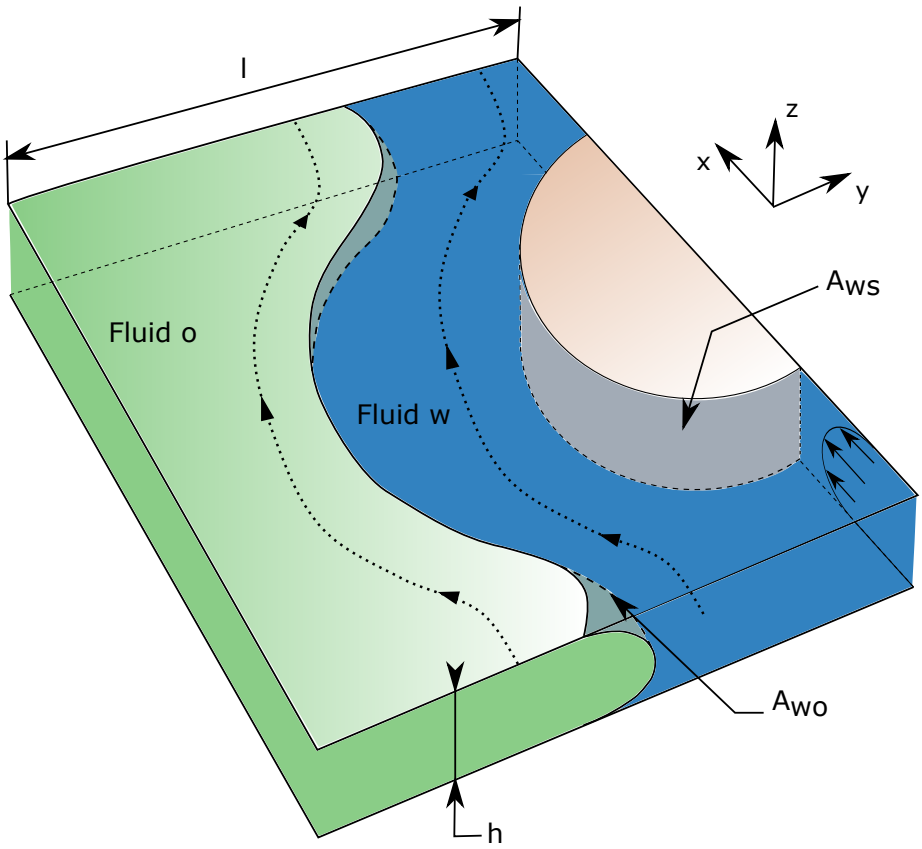

Figure 2: Illustation of confined cocurrent two-phase flow between two parallel plates and around cylinder obstacles.

Beside the interface curvature in the Hele-Shaw cell plane, the meniscus in the perpendicular plane must be taken into account. Therefore, the pressure jump at equilibrium across the interface reads

$$\Delta p = \gamma \left(\frac{2}{h} + \kappa_{\parallel} \right), \tag{13}$$

where γ denotes the surface tension and $\kappa_{\parallel}$ the curvature in the Hele-Shaw plane [35]. The eq. 13 was completed in [36] by an additional term that pertains for dynamic film formation and a corrective $\pi/4$ factor for the curvature in the cell plane.

To compute the traction exerted by the fluids on the cell plates we need to consider that the velocity profile in the z-direction is well described by the Poiseuille flow profile,

$$u = -\frac{1}{2\mu} \frac{dp}{dx} z(z-h). \tag{14}$$

Then the friction force exerted on the bottom plate is given by

$$\mu \frac{\partial u}{\partial z} \mid_{z=0} = -\frac{h}{2} \frac{dp}{dx}. \tag{15}$$

Thus, the traction $T^x_{i,pl}$ is obtained by multiplying the friction force by two times the surface wetted by the fluid i.

We can show that the average velocity taken over the interval between the plates is written as follows

$$\mathbf{U}(x, y, 0) = -\frac{h^2}{12\mu} \nabla_{\parallel} p. \tag{16}$$

There is therefore a direct analogy between flows in a 2D porous medium and a flow in a Hele-Shaw cell, as can be seen in eq. 16, where the permeability is given by $h^2/12$ [35].

Direct numerical simulations

Equations

Level Set model

We use the Level Set method to capture the moving free interface between the fluids. In this framework the fluid phases are identified with a level set (scalar) function that goes smoothly from 0 to 1 across the fluid interface and the interface is implicitely defined as the iso-level $\phi = 0.5$. The transport of the level set function ϕ is governed by

$$\frac{\partial \phi}{\partial t} + \nabla \cdot (\mathbf{u}\phi) = \tau \nabla \cdot \left(\psi \boldsymbol{\nabla} \phi - \phi(1-\phi) \frac{\boldsymbol{\nabla} \phi}{|\nabla \phi|} \right). \tag{17}$$

In this equation, $\mathbf{u}$ is the velocity field, τ and ψ are two numerical parameters that control the diffuse interface thickness and the amount of reinitialization of the ϕ function, respectively [37,38].

Flow model

Remember that we need to take into account tangential stress as well perpendicular stress due to the flow confinement, a full-3D resolution of the flow equations would be meaningful. In order to avoid solving such resource-intensive simulations we rather resolved 2D flow equations plus an additional term taking into account the perpendicular stress. The velocity and pressure fields are obtained by solving the 2D-modified Stokes equations since the Reynolds number is assumed

to be sufficiently low so that the flow is creeping, the whole-domain formulation Stokes and continuity equations read

$$0 = -\nabla p + \mu(\phi)\left(\nabla^2 \mathbf{u} - k^2 \mathbf{u}\right) + \mathbf{F}_{st}, \tag{18}$$

$$0 = \nabla \cdot \mathbf{u}, \tag{19}$$

where $k = \frac{\sqrt{12}}{h}$ is an additional term that pertain to a Darcy-term arising from the depth-averaging of the Stokes equation, as described in the theoretical background section and $\mathbf{F}_{st}$ is the capillary contribution. The capillary contribution is difficult to compute in volumetric methods such as Level Set and is itself the object of a large body of work [39], this term is defined here as

$$\mathbf{F}_{st} = \gamma \kappa \delta(\phi) \mathbf{n}, \tag{20}$$

where γ is the surface tension, κ is the interface mean curvature, $\mathbf{n}$ denotes the unit normal to the interface and $\delta(\phi)$ is the Dirac delta function localized on the interface [40]. In this framework the unit normal vector as well as the mean curvature are obtained with the level set function ϕ as

$$\mathbf{n} = \frac{\boldsymbol{\nabla}\phi}{|\boldsymbol{\nabla}\phi|},$$

$$\kappa = \frac{\pi}{4} \nabla \cdot \left(\frac{\boldsymbol{\nabla}\phi}{|\boldsymbol{\nabla}\phi|} \right) + \kappa_{\perp},$$

respectively, where the $\pi/4$ correction was derived in [36] and $\kappa_{\perp} = \frac{2}{h}$ is the out-of-plane curvature as described previously in the theoretical background

section.

The material parameters, that is the fluid density and the fluid viscosity, varies smoothly from one fluid to another

$$\rho(\phi) = \rho_o + (\rho_w - \rho_o)\phi,$$

$$\mu(\phi) = \mu_o + (\mu_w - \mu_o)\phi.$$

Dimensionless equations and relevant dimensionless numbers

If one define the following dimensionless variables

$$\mathbf{u} = \mathbf{u}' \times U,\ p = p' \times \frac{\mu U}{l},\ \kappa = \kappa' \times l,\ \mathbf{x} = \mathbf{x}' \times l,$$

where U is a reference velocity, μ a reference viscosity and l a reference length, Stokes and continuity equations can be recast as

$$0 = -\nabla' p' + \frac{\mu(\phi)}{\mu}\nabla'^2\mathbf{u}' + \frac{\gamma}{\mu U}\kappa'\nabla'\phi,$$

$$0 = \nabla' \cdot \mathbf{u}'.$$

One can notice the two following dimensionless numbers

$$\bar{\mu} = \frac{\mu(\phi)}{\mu},\ Ca^{-1} = \frac{\gamma}{\mu U},$$

the viscosity ratio and the capillary number, respectively, which add up to the

already identified aspect ratio h/l.

Test case

Geometry and boundary conditions

We study a model system consisting of an array of cylinders in a thin square cuboid, resembling a Hele-Shaw-cell with obstacles, as shown in fig. 3. The two fluids are injected from the left at a constant normal velocity. The outlet boundary condition for the flow is a constant pressure. Initially the wetting fluid occupy the entire model as depicted in fig. 3. The different boundary conditions are listed in table 1.

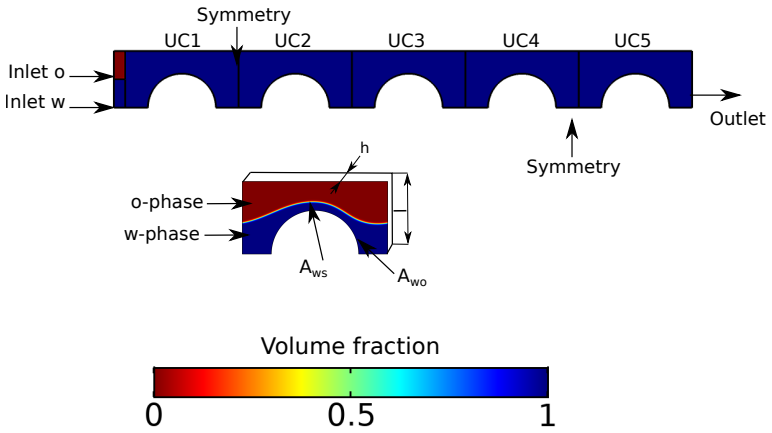

Figure 3: The geometry used is an array of 5 cylinders in a thin square cuboid, resembling a Hele-Shaw-cell where both fluids are injecting from left to right, initially the square cuboïd are saturated with wetting fluid (in blue), the length of one Unit-Cell (UC) is one millimetre.

Table 1: Boundary conditions used.

Boundary	u	p	ϕ
A_{ws}	0	-	$\mathbf{n} \cdot \mathbf{u}\phi = 0$
Outlet	-	0	$\mathbf{n} \cdot \boldsymbol{\nabla}\phi = 0$
Inlet o	$U_o^x = \text{cst}$	-	0
Inlet w	$U_w^x = \text{cst}$	-	1

Validation

Results

The results are given as a function of the dimensionless numbers defined previously. The reference length l is the width of the unit cells (0.5 mm), the reference viscosity is the invading fluid viscosity that is two times greater ($\mu_o = 2 \times 10^{-3}$ Pa.s) than the wetting fluid viscosity. and the reference velocity is the total velocity, that is $U = U_o + U_w$. In consequence the capillary number and the dimensionless inlet velocity read

$$Ca = \frac{(U_o + U_w)\mu_o}{\gamma},\ U_w^{'} = \frac{U_w}{U_o + U_w} = f_f,\ U_o^{'} = 1 - f_f,$$

respectively, where f_f is the fractional flow. In the following the viscosity ratio $\bar{\mu}$ as well as the fractional flow f_f are kept constant at 2 and 0.25, respectively.

In the following, the intrinsic permeability of the model is varied by modifying the aperture between the two plates of the cell. We use five different values for the aperture and the correspondence in terms of intrinsic permeability is given in table 2 from single-phase simulation. When $h \to \infty$, it is expected that the

intrinsic permeability tends towards the permeability obtained with purely 2D flow equations, this can be verified in fig. 4.

Table 2: Equivalence between the value of the cell plates aperture and the intrinsic permeability of the model obtained either from the intrinsic permeability for flow between two plates or from single-phase simulation in our model.

l/h	$h^2/12$ (darcy)	k Simulation (darcy)
0.2	5.21×10^5	1.48×10^4
2.0	5.21×10^3	2.85×10^3
4.0	1.30×10^3	8.63×10^2
8.0	3.26×10^2	2.35×10^2
20	5.21×10^1	3.94×10^1

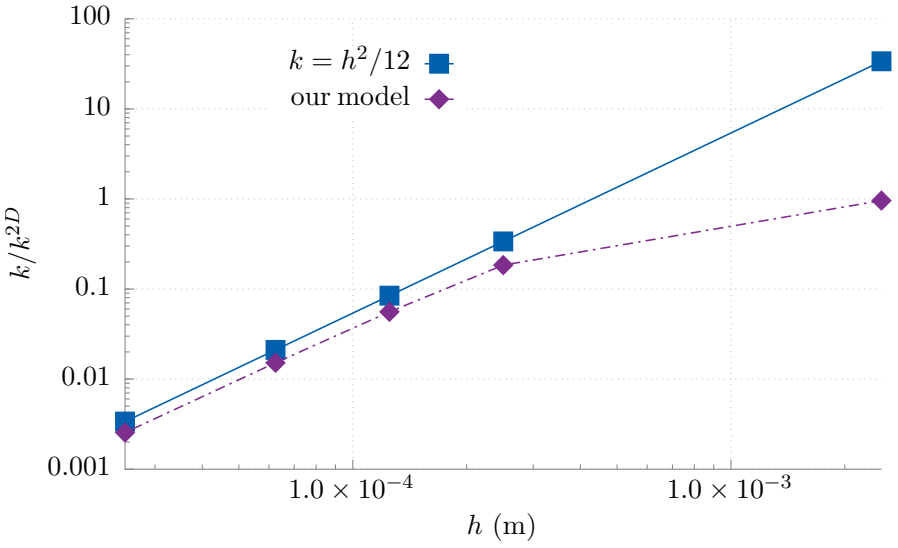

Figure 4: Intrinsic permeability of the Hele-Shaw cell normalized by the intrinsic permeability obtained from pure 2D simulation.

Wetting fluid saturation decreases when permeability is decreasing

Before we turn to the study of traction terms it is worth invesigate the effect of varying permeability on the fluid repartition and the velocity fields. Wetting fluid saturation in the third unit-cell (UC3), computed accordingly to eq. 10, is given as a function of the dimensionless aperture between the plates in fig. 5.

The wetting fluid saturation non-linearly decreases with h^* and stays at moderate values, between 0.6 and 0.3. A smaller capillary number tends to slightly increase the wetting fluid saturation at steady-state.

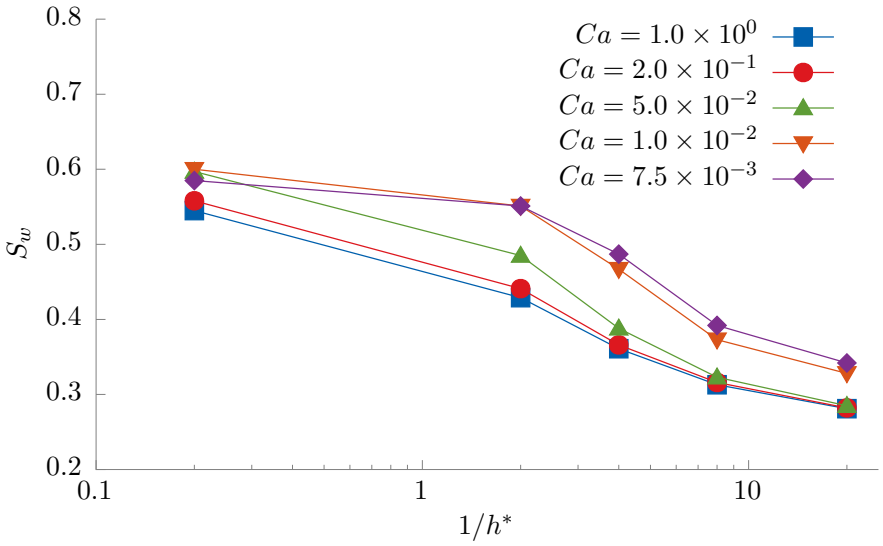

Figure 5: Saturation in wetting fluid as a function of the dimensionless aperture $h^* = h/l$ and for different values of the capillary number (UC3) at steady-state.

Let us take a closer look at the interface position for different values of h^* for $Ca = 1$ and $Ca = 0.05$ in fig. 6 and fig. 7, respectively. The interface for small capillary number and large aperture is significantly flatter than for high capillary number and/or small aperture. One also noted that the interface is symmetrical when the capillary number is large whereas it loses this property for a smaller

capillary number and for larger aperture between the plates. On the same plots we show the position of the interface in a purely 2D case, and one can see that it is very close to the solution for $1/h^* = 0.2$. The fluid-fluid interface moves closer to the cylinder for decreasing aperture (i.e. intrinsic permeability), this has an impact on the velocity fields, as shown in fig. 8 and fig. 9, which represent the dimensionless x-component of the velocity for $Ca = 1.0$ and $1/h^* = 2$ and $1/h^* = 20$, respectively. Clearly, what is happening here is that the velocity profile is close to the Poiseuille profile as long as the interface is not too close from the solid. To verify this, we plot in fig. 10 the dimensionless x-component of the velocity along the line shown in fig. 9. The profile for the pure 2D solution ($h \to \infty$) resembles a Poiseuille profile while for decreasing aperture the maximum velocity is observed between the solid and the fluid-fluid interface.

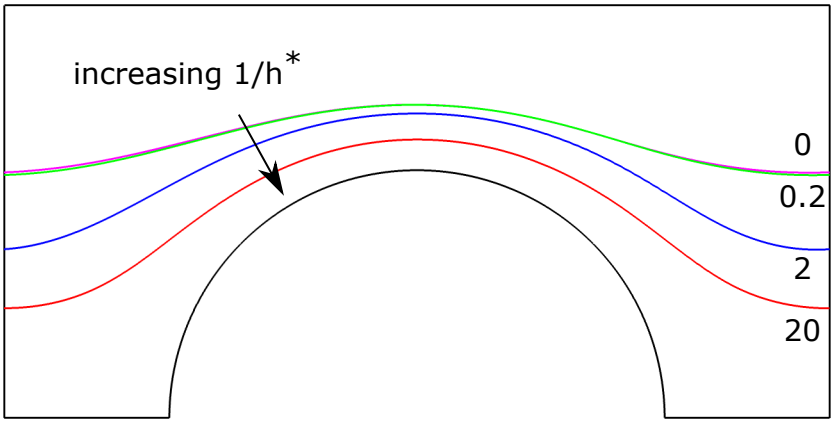

Figure 6: Interface position at steady-state in UC3 for $Ca = 5 \times 10^{-2}$.

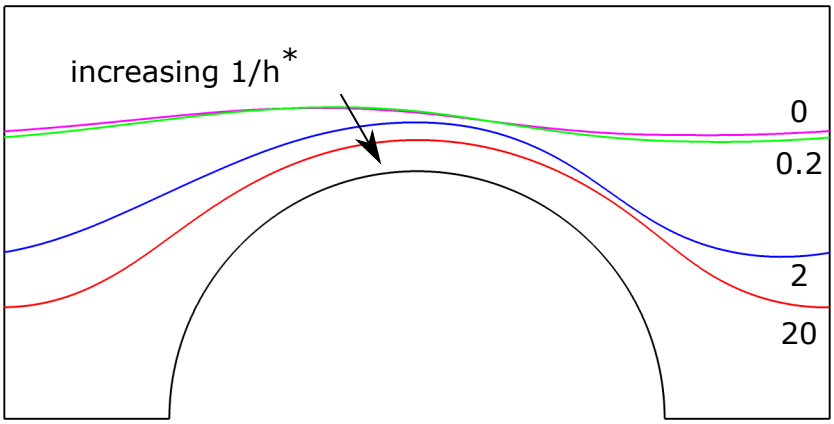

Figure 7: Interface position at steady-state in UC3 for $Ca = 5 \times 10^{-2}$.

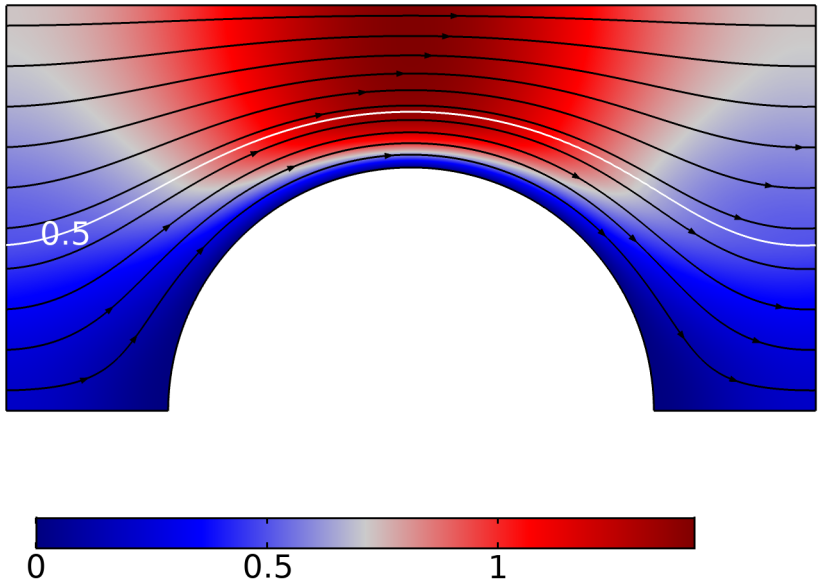

Figure 8: Dimensionless x-component of the velocity in UC3 for $Ca = 1$ and $1/h^* = 2$.

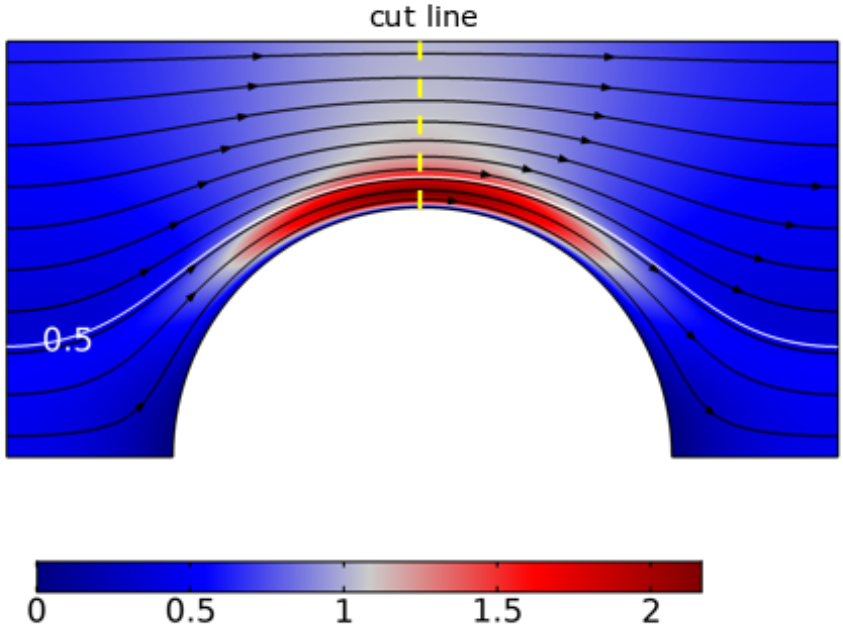

Figure 9: Dimensionless x-component of the velocity in UC3 for $Ca = 1$ and $1/h^* = 20$.

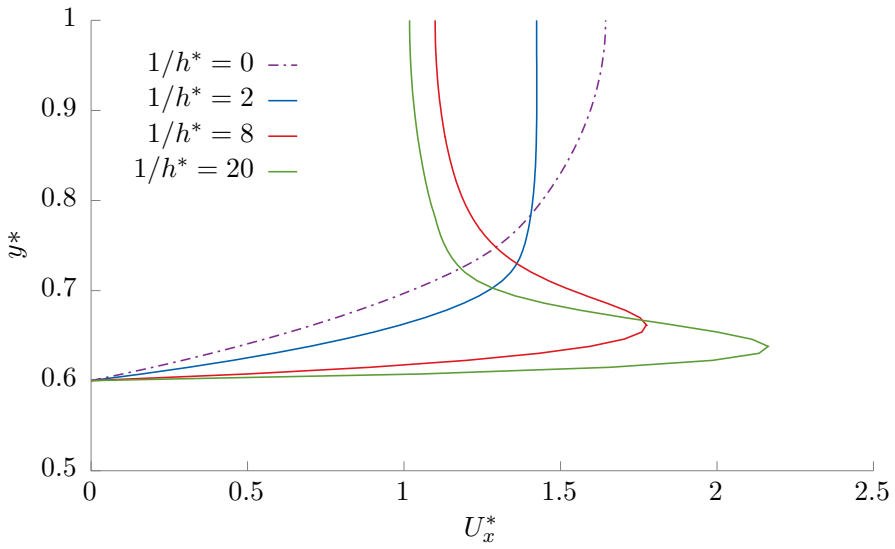

Figure 10: Dimensionless x-velocity profile in UC3 for $Ca = 1$ and different values of the intrinsic permeability.

Dynamic capillary pressure scale linearly with the gap between Hele-Shaw plates regardless of the capillary number

We now consider the dynamic capillary pressure as defined in eq. 12 as a function of h^*. As can be seen on fig. 11, P_c perfectly scales linearly with h^*, regardless of the capillary number. One can find on the same plot the theoretical pressure jump across the fluid-fluid interface due to the out-of-plane meniscus. This pressure jump closely matches the computed dynamic capillary pressure and to this point, we can conclude that even for the largest aperture the difference of mean intrinsic pressure is given by the meniscus between the two plates. Seeing this, it is worthwhile to contrast the pressure jump across the interface with the pressure gradient across the cell. We plot the pressure field in the third unit-cell (UC3) for $Ca = 1$ and $1/h^* = 2$ on **??** (a) and $1/h^* = 20$ on **??** (b), and one can note that, although the pressure jump is greater in absolute terms, it is almost unobservable for the smallest aperture because of the large pressure gradient.

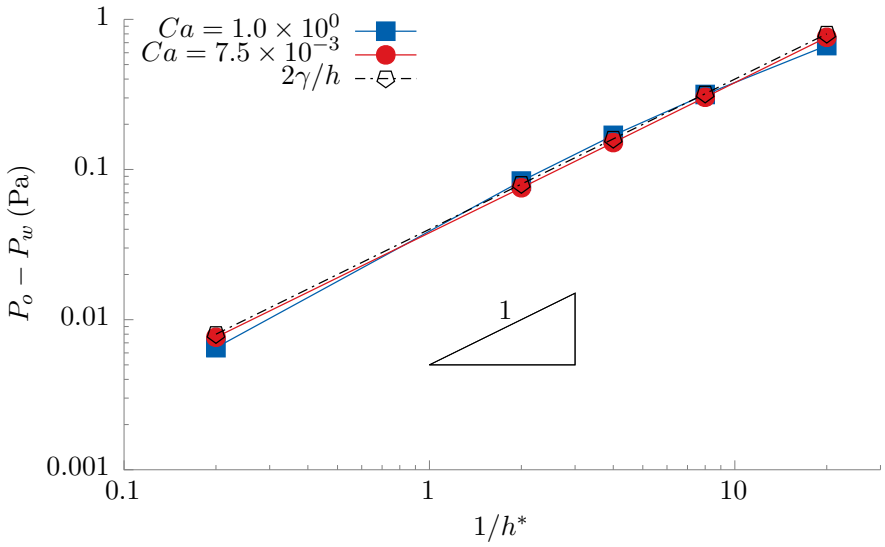

Figure 11: Dynamic capillary pressure in UC3 as a function of h^* for different capillary numbers and pressure drop across the fluid-fluid based on the out-of-plane meniscus at steady-state

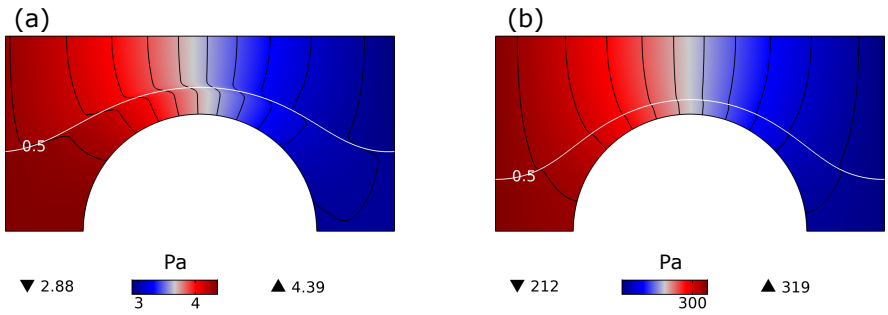

Figure 12: Pressure field in UC3 for $Ca = 1$ and (a) $1/h^* = 2$ and (b) $1/h^* = 20$ and interface position as the iso-ϕ=0.5 contour

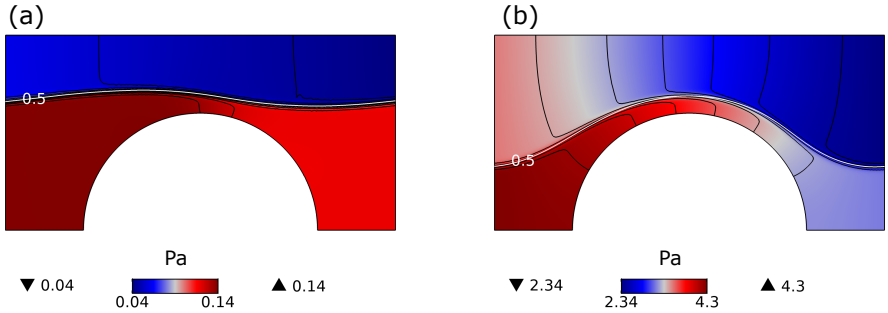

Figure 13: Pressure field in UC3 for $Ca = 1 \times 10^{-2}$ and (a) $1/h^* = 2$ and (b) $1/h^* = 20$ and interface position as the iso-ϕ=0.5 contour

Fluid-fluid traction increases faster compared to solid-fluid traction when permeability is decreasing

Here we plot each traction terms as a function of the aperture of the Hele-Shaw plates (i.e. intrinsic permeability). We have identified three boundaries, namely the fluid-fluid boundary S_{ow}, the fluid-plates boundary $S_{i,pl}$ and the fluid-cylinder boundary $S_{w,cyl}$. We first plot on fig. 14 traction exerted on the Hele-Shaw plates by each fluid, remember that this term is computed as described in the theoretical background section. It is meaningful that the traction exerted by the non-wetting fluid on the cell plates becomes more important for smaller aperture

since, as discussed above, the surface wetted by this fluid becomes larger as the aperture decreases.

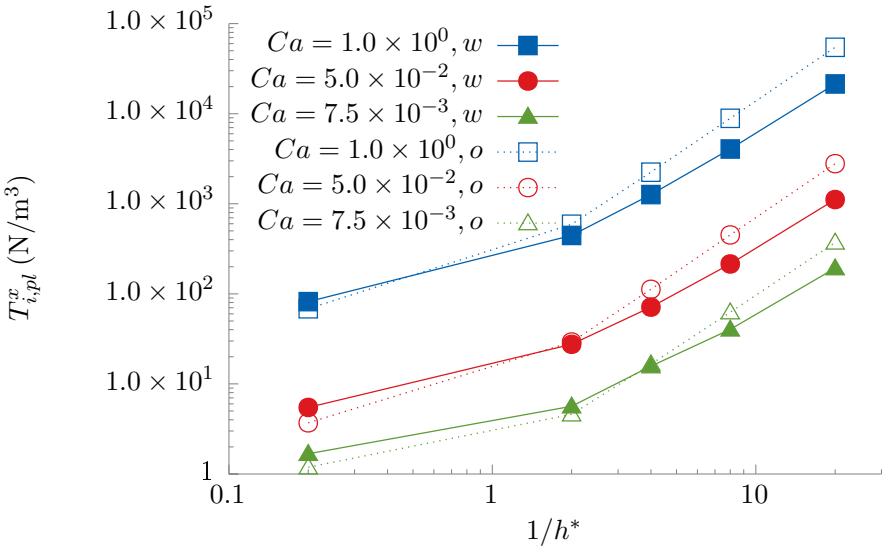

Figure 14: x-component of the traction on Hele-Shaw cell plates by each fluid in UC3, as a function of the dimensionless gap and for different capillary numbers at steady-state.

In fig. 15 we plot the sum of traction (x-component) exerted on all solid-fluid boundaries as a function of the dimensionless aperture between the plates and for different capillary numbers. For $1/h^*$ greater than 2, the traction scale a bit slower than $1/h^2$. Logically, the greater the capillary number, the greater the traction term.

We compute the fluid-fluid traction T_{ij} in two steps. The first step concerns the viscous part of the stress tensor, which is calculated directly from the velocity gradients available on the interface contour. The second step concerns the pressure part, which is obtained by applying the divergence theorem on each phase into UC3. In fig. 16 we plot the traction on the fluid-fluid interface T_{ow} as a function of $h*$. Starting from $1/h^* = 2$ the traction scale a bit faster than

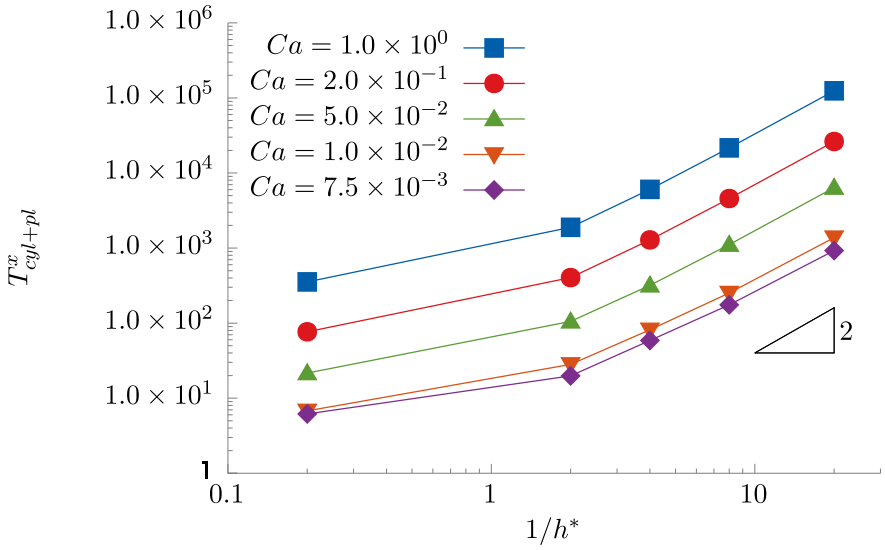

Figure 15: x-component of the traction exerted on the cylinder in UC3 as a function of the dimensionless aperture and for different capillary numbers at steady-state.

$1/h^2$. We now return to the traction on solid/fluid boundaries and it can be seen that the latter is greater, but by less than one order of magnitude, than the traction on the fluid-fluid interface.

Decreasing the permeability does not imply that the share of the fluid-fluid traction is negligible in the total traction

Let us now sum up all the traction terms and answer the question of the share of traction exerted on the fluid-fluid interfaces in total traction. The ratio T^x_{ij}/T^x_s, with $s = pl + cyl$, is given as a function of the dimensionless gap between the Hele-Shaw plates in fig. 17. In our results the traction at the fluid-fluid interfaces reaches between 5 to 30% of the traction exerted on the interfaces between fluid and solid and the ratio varies non-monotonically with h^*, the minimum being reached for the smallest capillary numbers and an intermediate gap between the

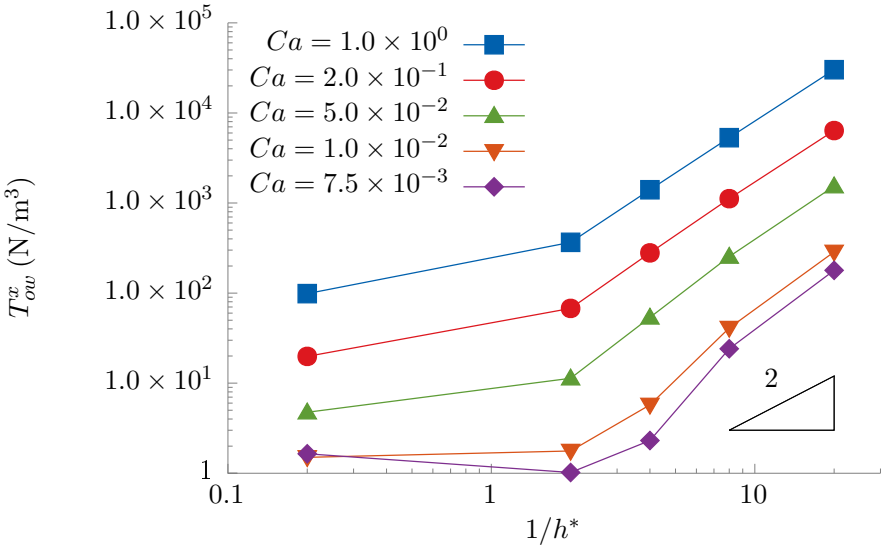

Figure 16: x-component of the traction exerted on the fluid-fluid interface in UC3 as a function of the dimensionless aperture and for different capillary numbers at steady-state.

plates.

Discussion

[1] Fetter CW, Boving T, Kreamer D. Contaminant hydrogeology. Waveland Press; 2017.

[2] Clavier R, Chikhi N, Fichot F, Quintard M. Modeling of inertial multiphase flows through high permeability porous media: Friction closure laws. International Journal of Multiphase Flow 2017;91:243–61.

[3] Santos JM de, Melli TR, Scriven LE. Mechanics of gas-liquid flow in packed-bed contactors. Annual Review of Fluid Mechanics 1991;23:233–60. https://doi.org/10.1146/annurev.fl.23.010191.001313.

[4] Davit Y, Quintard M. One-phase and two-phase flow in highly permeable

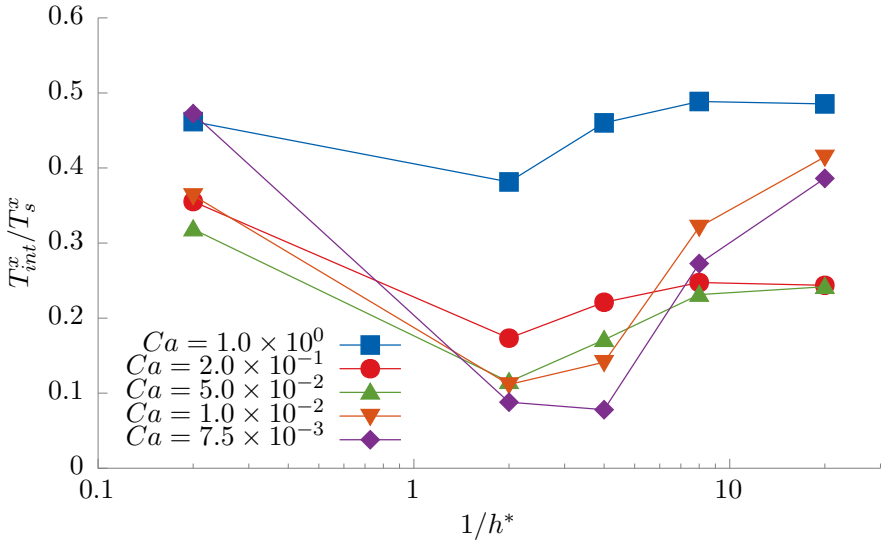

Figure 17: Ratio of traction on fluid-fluid interface over traction on sloid-fluid interfaces in UC3 as a function of the gap between the Hele-Shaw plates and for different capillary numbers at steady-state.

porous media. Heat Transfer Engineering 2018:1–19.

[5] Dullien FAL. Porous media: Fluid transport and pore structure. Academic press; 2012.

[6] Avraam DG, Payatakes AC. Flow regimes and relative permeabilities during steady-state two-phase flow in porous media. Journal of Fluid Mechanics 1995;293:207–36. https://doi.org/10.1017/S0022112095001698.

[7] Armstrong RT, McClure JE, Berrill MA, Rücker M, Schlüter S, Berg S. Beyond darcy's law: The role of phase topology and ganglion dynamics for two-fluid flow. Physical Review E 2016;94:043113.

[8] Wyckoff RD, Botset HG. The flow of gas-liquid mixtures through unconsolidated sands. Physics 1936;7:325–45.

[9] Muskat M. The flow of homogeneous fluids through porous media. Soil

Science 1938;46:169.

[10] Leverett M, others. Capillary behavior in porous solids. Transactions of the AIME 1941;142:152–69.

[11] Kalaydjian F-M, others. Dynamic capillary pressure curve for water/oil displacement in porous media: Theory vs. Experiment. In:. SPE annual technical conference and exhibition, Society of Petroleum Engineers; 1992.

[12] Hassanizadeh SM, Gray WG. Thermodynamic basis of capillary pressure in porous media. Water Resources Research 1993;29:3389–405. https://doi.org/10.1029/93WR01495.

[13] Barenblatt GI, Patzek TW, Silin DB. The mathematical model of nonequilibrium effects in water-oil displacement. SPE Journal 2003;8:409–16.

[14] Hilfer R. Macroscopic equations of motion for two-phase flow in porous media. Physical Review E 1998;58:2090.

[15] Blunt MJ. Multiphase flow in permeable media: A pore-scale perspective. Cambridge University Press; 2017.

[16] Marle CM. On macroscopic equations governing multiphase flow with diffusion and chemical reactions in porous media. International Journal of Engineering Science 1982;20:643–62. https://doi.org/https://doi.org/10.1016/0020-7225(82)90118-5.

[17] Whitaker S. Flow in porous media II: The governing equations for immiscible, two-phase flow. Transport in Porous Media 1986;1:105–25.

[18] Auriault J, Sanchez-Palencia E. Remarques sur la loi de darcy pour les écoulements biphasiques en milieu poreux. Journal of Theoretical and Applied Mechanics, Numéro Spécial 1986:p141–156.

[19] Kalaydjian F. Origin and quantification of coupling between relative permeabilities for two-phase flows in porous media. Transport in Porous Media 1990;5:215–29.

[20] Lasseux D, Quintard M, Whitaker S. Determination of permeability tensors for two-phase flow in homogeneous porous media: Theory. Transport in Porous Media 1996;24:107–37.

[21] Zarcone C, Lenormand R. Détermination expérimentale du couplage visqueux dans les écoulements diphasiques en milieu poreux. Comptes Rendus de L'Académie Des Sciences Série II, Mécanique, Physique, Chimie, Astronomie 1994;318:1429–35.

[22] Dullien FAL, Dong M. Experimental determination of the flow transport coefficients in the coupled equations of two-phase flow in porous media. Transport in Porous Media 1996;25:97–120. https://doi.org/10.1007/bf00141264.

[23] Ramakrishnan TS, Goode PA. Measurement of off-diagonal transport coefficients in two-phase flow in porous media. Journal of Colloid and Interface Science 2015;449:392–8.

[24] Rose W. Measuring transport coefficients necessary for the description of coupled two-phase flow of immiscible fluids in porous media. Transport in Porous Media 1988;3:163–71. https://doi.org/10.1007/BF00820343.

[25] Bentsen RG, Manai AA. On the use of conventional cocurrent and countercurrent effective permeabilities to estimate the four generalized permeability coefficients which arise in coupled, two-phase flow. Transport in Porous Media 1993;11:243–62.

[26] Langaas K, Papatzacos P. Numerical investigations of the steady state relative permeability of a simplified porous medium. Transport in Porous Media

2001;45:241–66.

[27] Avraam DG, Payatakes AC. Generalized relative permeability coefficients during steady-state two-phase flow in porous media, and correlation with the flow mechanisms. Transport in Porous Media 1995;20:135–68. https://doi.org/10.1007/bf00616928.

[28] Rothman DH. Macroscopic laws for immiscible two-phase flow in porous media: Results from numerical experiments. Journal of Geophysical Research 1990;95:8663. https://doi.org/10.1029/jb095ib06p08663.

[29] Li H, Pan C, Miller CT. Pore-scale investigation of viscous coupling effects for two-phase flow in porous media. Physical Review E 2005;72. https://doi.org/10.1103/physreve.72.026705.

[30] Yiotis AG, Psihogios J, Kainourgiakis ME, Papaioannou A, Stubos AK. A lattice boltzmann study of viscous coupling effects in immiscible two-phase flow in porous media. Colloids and Surfaces A: Physicochemical and Engineering Aspects 2007;300:35–49. https://doi.org/https://doi.org/10.1016/j.colsurfa.2006.12.045.

[31] Odeh AS, others. Effect of viscosity ratio on relative permeability (includes associated paper 1496-g) 1959.

[32] Shams M, Raeini AQ, Blunt MJ, Bijeljic B. A study to investigate viscous coupling effects on the hydraulic conductance of fluid layers in two-phase flow at the pore level. Journal of Colloid and Interface Science 2018;522:299–310.

[33] Whitaker S. The method of volume averaging. vol. 13. Springer Science & Business Media; 2013.

[34] Kalaydjian F. A macroscopic description of multiphase flow in porous media involving spacetime evolution of fluid/fluid interface. Transport in Porous Media 1987;2:537–52. https://doi.org/10.1007/BF00192154.

[35] Saffman PG, Taylor GI. The penetration of a fluid into a porous medium or hele-shaw cell containing a more viscous liquid. Proceedings of the Royal Society of London Series A Mathematical and Physical Sciences 1958;245:312–29.

[36] Park C-W, Homsy G. Two-phase displacement in hele shaw cells: Theory. Journal of Fluid Mechanics 1984;139:291–308.

[37] Olsson E, Kreiss G. A conservative level set method for two phase flow. Journal of Computational Physics 2005;210:225–46. https://doi.org/https://doi.org/10.1016/j.jcp.2005.04.007.

[38] Olsson E, Kreiss G, Zahedi S. A conservative level set method for two phase flow ii. Journal of Computational Physics 2007;225:785–807. https://doi.org/https://doi.org/10.1016/j.jcp.2006.12.027.

[39] Popinet S. Numerical models of surface tension. Annual Review of Fluid Mechanics 2018;50:49–75. https://doi.org/10.1146/annurev-fluid-122316-045034.

[40] Galusinski C, Vigneaux P. On stability condition for bifluid flows with surface tension: Application to microfluidics. Journal of Computational Physics 2008;227:6140–64. https://doi.org/https://doi.org/10.1016/j.jcp.2008.02.023.